applied sciences

Article

Unity Power Factor Operation in Microgrid Applications Using Fuzzy Type 2 Nested Controllers

Hilmy Awad [1], Amr M. Ibrahim [2], Michele De Santis [3,*] and Ehab H. E. Bayoumi [4]

1 Department of Electrical Technology, Faculty of Technology and Education, Helwan University, Cairo 11715, Egypt; hilmy_awad@techedu.helwan.edu.eg
2 Department of Electrical Power and Machines Engineering, Ain Shams University, Cairo 11517, Egypt; amr_rizk@eng.asu.edu.eg
3 Department of Engineering, Niccolò Cusano University, 00166 Roma, Italy
4 Department of Mechanical Engineering, Faculty of Engineering, The British University in Egypt (BUE), El Sherouk, Cairo 11837, Egypt; ehab.bayoumi@bue.edu.eg
* Correspondence: michele.desantis@unicusano.it

Featured Application: This work introduces a Fuzzy-Type-2 controller to address the issue of the low-power factor operation of microgrids. The power factor is an essential index for economic and technical operations. The proposed method can be applied to improve the power factor in microgrids using deterministic optimization to obtain the controller parameters.

Abstract: The issue of low-power factor operation microgrids was reported for several layouts. Although numerous power factor improvement strategies have been applied and tested, various concerns remain to be addressed such as transient performance, simplicity of implementation, and satisfying the power-quality standards. The presented research aimed to design and implement controllers that can improve the transient response of microgrids due to changes in the load demand and achieve a near-unity power factor at the AC grid side, to which the DC microgrid is connected. Due to the nonlinear nature of microgrids, as they rely on power electronics converters, a Fuzzy type 2 controller was designed, implemented, and tested. The focus was given to improving the power factor of the DC microgrids. The validation of the proposed technique was verified by comparing its performance with Fuzzy type 1 and autotuned conventional PI controllers. To achieve the set aims, two nested control loops were designed with an inner current loop and an outer voltage loop. Besides MATLAB/Simulink simulations, a 10 kHz-sampling dSPACE platform was used to implement the suggested system. Two operational scenarios were tested: (1) a step change in the DC link voltage and (2) a change in the AC load (increase and decrease) at the output of the power inverter, connected to the DC grid. The simulation and experimental results confirmed that the proposed Fuzzy type 2 controller performed better than the other two techniques regarding the dynamic response, steady-state error, and compliance with power quality standards. Conventional approaches develop controllers using a linearized model, which limits the model accuracy and ignores higher-order variability. The method employs the nonlinear model. Fuzzy type 2 can better approximate high-precision problems than Fuzzy type 1.

Keywords: boost converter; Fuzzy type 2; microgrids; unity power factor

Citation: Awad, H.; Ibrahim, A.M.; De Santis, M.; Bayoumi, E.H.E. Unity Power Factor Operation in Microgrid Applications Using Fuzzy Type 2 Nested Controllers. *Appl. Sci.* **2023**, *13*, 5537. https://doi.org/10.3390/app13095537

Academic Editor: Hannu Laaksonen

Received: 3 April 2023
Revised: 28 April 2023
Accepted: 28 April 2023
Published: 29 April 2023

1. Introduction

Microgrids (MGs) are replacing remote central station power plants with localized, distributed generation, especially in cities, towns, and campuses [1]. MGs are durable and can supply competitive services due to their ability to operate in three distinct modes: on the grid, islanded, and autonomous [2]. Moreover, they provide positive social and environmental impacts globally [3]. However, the proliferation of MGs contributes to power quality problems at the distribution level [4]. One of these problems is the poor power factor and its measurements [4,5].

The power factor is an essential index for economic and technical operations. Low power factor implies overloading of electrical equipment and might cause unnecessary tripping. It is well-known that electrical motors consume a significant fraction of the delivered electrical energy. Among the electrical motors, induction motors, either three-phase or single-phase, are the most common due to their merits such as being relatively cheap, rugged, and maintenance-free. However, induction motors draw current with a low power factor, particularly at medium and light loading conditions. For a 200-hp, three-phase induction motor, the low power factor operation cost was $7888 per year [6].

Therefore, continuously improving the power factor is highly desirable, which ultimately enhances the system's power quality. Many techniques and system configurations have been reported in the literature to enhance the power quality of induction-motor drives. For instance, 12- and 24-pulse AC to DC rectifiers were proposed and tested in [7] to improve the power up to 0.936 at full load. However, in such a system, the existence of the phase shift transformer causes the system to be bulky and expensive. An AC chopper with four switches and applying the hysteresis-band control was reported in [8]. Although the tested configuration in [8] is simple and cost-effective, the flexibility to control the speed or torque of the induction motor might be limited, and there is always a need to transfer between control modes to achieve a power factor improvement.

To increase the system's power factor, ref. [9] presents a 9-switch AC–DC–AC converter that inserts a leading reactive power at the point of common connection. Even though the reported simulation and experimental findings demonstrate the converter and control's efficiency, this setup is still susceptible to grid-side disturbances and asymmetrical operation of the converter switches. Furthermore, real-world use requires an analysis of the switching losses, projected to be slightly larger than those of alternative systems.

Various switching control approaches based on pulse-width modulation (PWM) have been used for the boost converter to increase its responsiveness while keeping it stable. Proportional integral derivative control is the most widely used PWM switching control method because of its ease of use. Voltage and current must have a dynamic response. Hence, double-loop control is required. Utilizing a model-based compact form, formulations in the design of a double-loop PI-based, the DC–DC boost converter controller produced excellent system responses to parameter variations and disturbances [10].

Sliding mode control is a robust closed-loop method for unpredictable and disturbed plants. One sliding surface makes a sturdy controller and removes inductor current measuring. A control scheme with a hysteresis loop prevented chattering caused by sliding mode control discontinuities [11]. Because it may approach any function by learning the system process, neural network control is ideal for nonlinear control systems and working with uncertainties and incomplete information [12]. Online learning strategies have been developed to increase neural network control performance. The neural network control produced better overshoot, oscillation, settling time, and fast response to track the required output voltage [13].

Fuzzy logic control (FLC) is a form of intelligent control that does not necessitate elaborate mathematical modeling or calculations. Fuzzy logic controller design allows for dynamic small and big signal performance that is unachievable with linear control methods [9] and enhances the limits on overshooting and the sensitivity to parameter changes [14,15]. Fuzzy type 1 and type 2 were compared in studies such as [16,17]. The findings of the comparisons indicate that type-2 fuzzy logic controllers can provide superior control in terms of robustness [16,17].

Most studies have designed fuzzy-based energy management systems for grid-connected or islanded MGs by adjusting the FLC parameters through meta-heuristic algorithms. The authors in [18] performed an energy management system for a MG considering photovoltaic (PV) and wind turbine (WT) systems, battery energy storage systems, and a dynamic electricity cost profile during the day. The results demonstrate the efficacy of the proposed methodology in terms of saving on electricity bills. In [19], the fuzzy-based energy management system study was more focused on ensuring the safe and economical operation of the MG. This last study did not show any optimization of the parameters of the FLC. The authors in [20] used meta-heuristic methods to find the optimal parameters of the FLC to reduce power peaks and smooth the power flows exchanged with the main network in a grid-connected MG. In this area, the most widely used heuristic optimizations are the particle swarm optimization and the cuckoo search algorithms, as presented in [21].

Although these studies are very interesting, they consider the energy management aspect of the MG through FLC techniques and heuristic optimizations, and do not consider the technical aspects such as the power quality and deterministic optimizations.

This paper aims to fill this scientific gap by introducing a FLC method to improve the power factor in a DC MG, using deterministic optimization to obtain the controller parameters. To regulate the voltage and keep the current in phase with the source voltage, the boost converter and a cascade PI controller were used in this study. Each loop's transfer function calculates the controller gains, making the proposed controller a hybrid of an outer- and an inner-loop voltage- and current-control scheme.

The scientific improvements, compared to the present literature, introduced by this study are:

- The conventional methods design controllers based on a linearized model, which is limited to the model accuracy and does not consider higher-order variations. The proposed technique uses the nonlinear model directly.
- Compared to Fuzzy type 1, Fuzzy type 2 has a higher approximation capacity, making it a better choice for solving high-precision problems.
- The use of a deterministic optimization for the determination of the FLC parameters guarantees an optimal solution; the optimal result is not guaranteed with meta-heuristic optimization algorithms;
- The application of the FLC approach to power quality issues via DC MGs, whose application in the literature is rather limited, if not absent.

The rest of this paper is organized as follows. Section 2 presents the problem formulation, and Section 3 briefly describes the basics of Fuzzy type controllers. In Section 3, the proposed system is illustrated. The mathematical model of the proposed system is derived in Section 4. Section 5 presents the simulation and experimental results, while Section 6 states the research conclusions.

2. Problem Formulation

The MG has been innovated to fulfill the varying and dynamic needs of DC and AC loads. Other advantages include improved power management and stable performance [22]. The MG solves source and load compatibility difficulties and integrates energy sources and consumer loads with minimal conversion stages [23]. However, the problem of low power factor has been reported for many MG systems such as maritime MGs [24], MGs employing three-phase three-wire grid-connected inverters [25], MGs utilizing thyristor-based compensation (series or shunt) [26,27], and AC MGs integrating wind-energy systems [28].

In [29], the authors proposed a review of the norms and standards used in MGs that should be used for the interconnection and disconnection of MGs in the downstream network. This study found the IEEE 1547 to be the most comprehensive standard. In [30], it was specified that distributed generators should always try producing at a unity power factor. Even if standards such as the IEEE 1547 state that the converter output power factor can be 0.85 lead/lag or higher, the inverters are typically designed to work with a unity power factor [31]. Considering the integration of distributed generators (DG) in the power system, the authors in [32] investigated power quality issues for a distribution system first modeled in PSCAD and then integrated with a photovoltaic, forming a MG power system. Each DG's power factor can also be determined by regulating both the frequency and voltage [33].

With this goal in mind, the authors of [34–36] exploited voltage regulation devices to improve the power quality in the MG configuration. They claimed that conventional reactive power compensators could not correct power factors, generally used as voltage regulating devices. They presented a novel strategy to use STATCOM devices to obtain the power factor correction in MG applications. Using regulation devices such as dynamic voltage restorers, the authors in [37] focused on the operation of unity power factor rectifier topology.

In similar MG structures, the study in [38] considered islanded inverter-based MGs (IBMGs) considering various load types; the authors proposed calculating the voltage sensitivity to the system loading in each bus based on the load power factor. Always considering the local loads, in [39], a novel artificial neural network (ANN)-based control approach was proposed to control the power quality as per the IEEE/IEC standards in MG systems. In [40], a strategy to improve the power factor at the point of common coupling (PCC) for MG applications was presented, and the proposed compensation scheme for power factor improvement can be used dynamically for linear and nonlinear loads. The performance of the smart load at different power factors was also evaluated in [41].

Although the techniques employed to improve the power factor in MGs, as described in Section 1, were implemented and tested, there are still many issues to be further elaborated on and considered. Among these issues are the accuracy in the steady state, the transient performance of the controllers, simplicity of implementation, and satisfying the power-quality standards of the amount of injected distortion. This paper presents a Fuzzy-type-2 based controller aiming to resolve such issues.

3. Proposed System

3.1. Fuzzy Type 2 Control

The use of FLC for a system is fundamentally based on rules derived from human skills and knowledge. Type 2 fuzzy sets (Fuzzy 2) are an enhanced version of ordinary fuzzy sets, namely, Fuzzy type 1 sets (Fuzzy 1) [42]. Expert knowledge of the problem should be used to define a knowledge base that includes information on the attribute values, fuzzy subsets identifying them, and the rules linking these variables to determine the output. The controller can analyze these outputs by fuzzifying the actual inputs and using the fuzzy control rules. Defuzzification transforms the fuzzy variables that are the intermediate results of evaluating fuzzy rules into non-fuzzy control information for the ultimate procedure [43]. Figure 1 groups the five primary components of a Fuzzy 2 logic set: Defuzzifier, Fuzzifier, Rules Base, and Type Reducer are all components of a Fuzzy inference engine. The controller receives its input from the clear deviations that can be seen between the measured outputs of the plant and its reference inputs. The outputs of the controller are precise control signals that are transmitted to the plant actuators. The determined plant outputs are forwarded to the fuzzy controller to alter the error input.

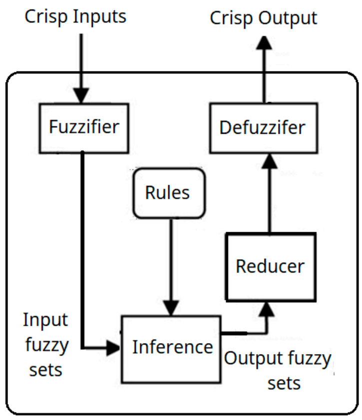

Figure 1. Regular Fuzzy 2 structure.

The fuzzy 2 controller has four fundamental elements:

1. Fuzzification is the layout that transforms input values from crisp to fuzzy. This operation allows us to determine the degrees to which each belonging function of each input applies to the fuzzy sets.
2. Linguistic rules contain human control problem knowledge. Expert knowledge is turned into logic to develop rule bases.
3. On the grounds of the knowledge base, an inference engine produces fuzzy controller inputs.
4. An interface for defuzzification that transforms fuzzy outputs into crisp outputs suitable for operating system actuators.

3.2. Layout of the Proposed System

The proposed system comprises a hybrid MG (HMG) that contains a DC MG, AC MG, and DC-link capacitor, as illustrated in Figure 2. The DC MG has two DG units, PV and fuel cell, battery bank, and DC loads. Each of them is linked to a DC/DC converter. The AC MG is tied to the DC MG via a diode rectifier and a boost DC/DC converter. There are also AC loads such as induction motor drives.

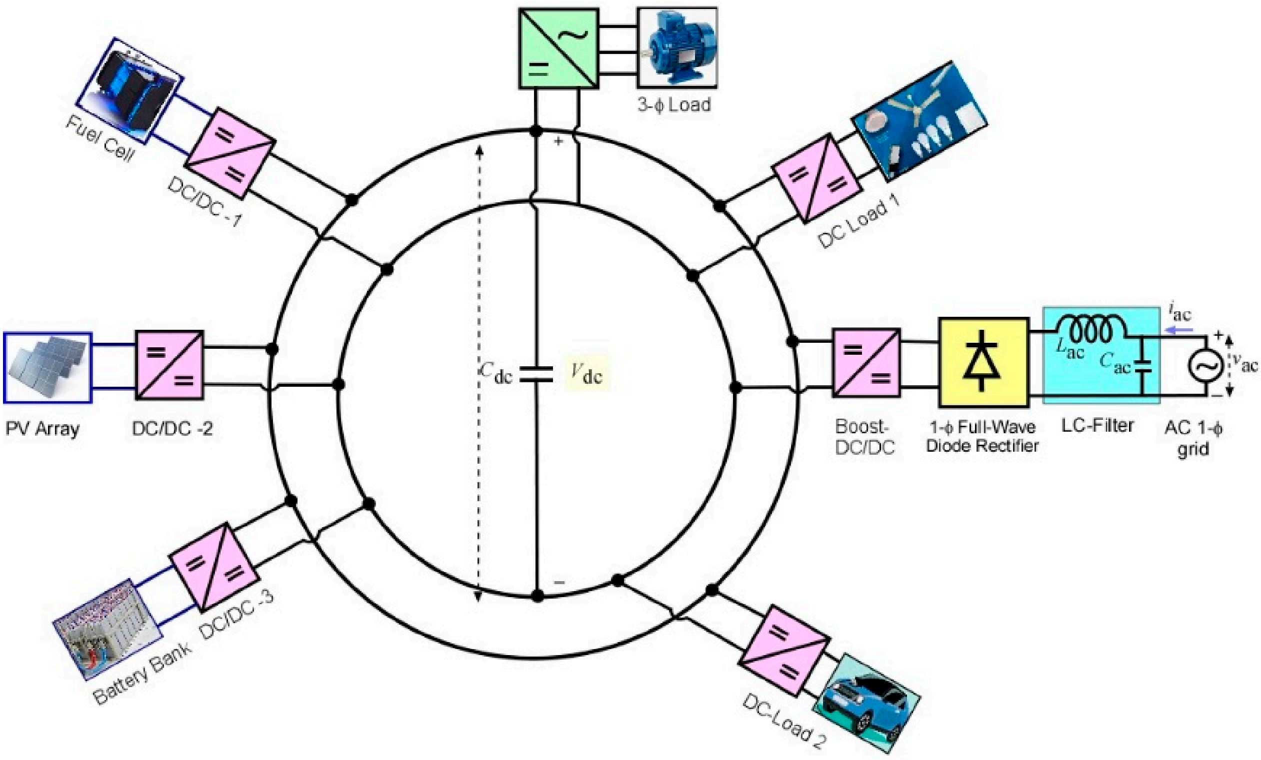

Figure 2. Layout of single-phase grid with DC microgrid and its DC loads.

As the scope of this article was the power factor improvement, the AC MG was modeled as a voltage source while the DC MG was modeled as a current source. This is depicted in Figure 3. The AC MG is mainly used as a backup if the DC MG generation does not satisfy the DC load requirements. The needed measurements are the rectified voltage v_b, rectified current i_b, the DC-link voltage $v_{dc,}$ and the DC-load current i_{dc}. The main aims of the proposed controller are: (1) compensate for the DC-link voltage variations due to load changes; (2) realize a near unity power factor for the AC MG; (3) ensure that the injected current satisfies the IEEE standards of harmonics. The control signal modulates the switch of the boost DC/DC converter to achieve the control goals.

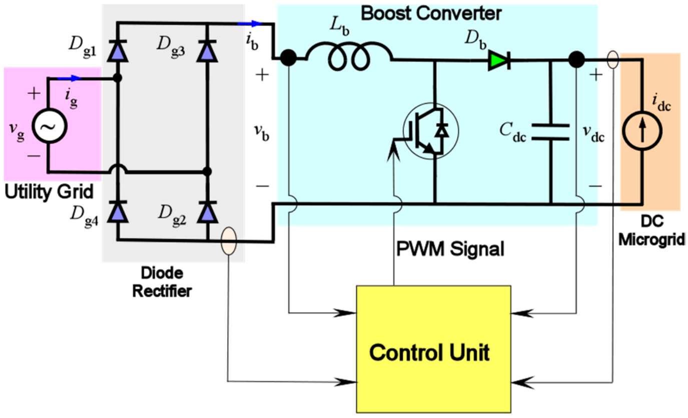

(a)

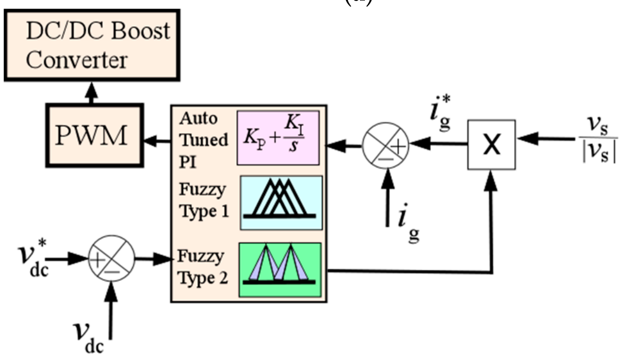

(b)

Figure 3. Single-phase grid model and DC boost converter control: (**a**) schematic diagram, and (**b**) control block diagram.

4. Mathematical Model

A. Diode Rectifier

$$i_b = |i_g| \tag{1}$$

$$v_b = |v_g| \tag{2}$$

B. Boost DC/DC Converter

If the switch is on:

$$\frac{d}{dt} i_b(t) = \frac{1}{L} v_b(t) \tag{3}$$

$$\frac{dv_c(t)}{dt} = -\frac{1}{C} i_{\mathrm{dc}}(t) \tag{4}$$

If the switch is off:

$$\frac{d}{dt} i_b(t) = \frac{1}{L} v_b(t) - \frac{1}{L} v_c(t) \tag{5}$$

$$\frac{dv_c(t)}{dt} = \frac{1}{C} i_b(t) - \frac{1}{C} i_{\mathrm{dc}}(t) \tag{6}$$

Averaging over one switching cycle yields:

$$\frac{d}{dt} i_b(t) = \frac{1}{L} v_b(t) - \frac{(1-d)}{L} v_c(t) \tag{7}$$

$$\frac{dv_c(t)}{dt} = \frac{(1-d)}{C} i_b(t) - \frac{1}{C} i_{\mathrm{dc}}(t) \tag{8}$$

4.1. Linear Model

The linearized model of the boost converter can be obtained by perturbing each variable, x, by an amount equal to Δx around a quiescent value X ignoring the higher-order terms; $x = X + \Delta x$.

For instance, $v_c(t) = V_c + \Delta v_c(t)$. Additionally, higher-order terms are neglected. The linearized model was obtained to design the parameters of the PI control and compare its performance against the Fuzzy 2 controller. The perturbed variables are:

$$v_c(t) = V_c + \Delta v_c(t) \tag{9}$$

$$v_b(t) = V_b + \Delta v_b(t) \tag{10}$$

$$i_b(t) = I_b + \Delta i_b(t) \tag{11}$$

$$i_{\mathrm{dc}}(t) = I_{\mathrm{dc}} + \Delta i_{\mathrm{dc}}(t) \tag{12}$$

$$d(t) = D + \Delta d(t) \tag{13}$$

Substituting Equations (9)–(13) into Equations (7) and (8) yields:

$$\frac{d}{dt}\Delta i_b(t) = \frac{1}{L}\{\Delta v_b(t) - (1-D)\Delta v_c(t) + V_c \Delta d(t)\} \tag{14}$$

$$\frac{dv_c(t)}{dt} = \frac{1}{C}\{(1-D)\Delta i_b(t) - I_b \Delta d(t) - \Delta i_{\mathrm{dc}}(t)\} \tag{15}$$

The nonlinear model of the system: Equations (1), (2), (7), and (8) were used in the design of the Fuzzy-2 controller, as explained in Section 3, while for the linear model, Equations (14) and (15) were exploited in the design of the PI controller.

4.2. Proposed Controller Design

Fuzzy controllers are designed for use in current and DC voltage loops. The fuzzy system's first and second inputs are the current/DC voltage error and its derivative. The triangle membership function was selected for the Fuzzy type 2 controller because it is simple to construct and produces good results with accepted precision.

There are seven linguistic tags to denote the entries: High Negative (HN), Medium Negative (MN), Low Negative (LN), Zero (Z), Low Positive (LP), Medium Positive (MP), and High Positive (HP). The following Member Functions (MFs) are used for the inputs: labels indicating HN and PH are trapezoidal, while those for MN, LN, Z, LP, and MP are triangles. Figure 4 depicts the input representing MFs.

The variability of the desired control is the fuzzy system's output. This output is denoted by 7-linguistic labels: Steep Drop (SD), Medium Drop (MD), Low Drop (LD), Zero (Z), Low Growth (LG), Medium Growth (MGH), and High Growth (HG). The MFs representing the output are shown in Table 1. The 49 rules needed to account for all possible inputs are based on the seven error (E) values and seven error change (ΔE) values. These are typically presented in Table 2.

Table 1. Output memberships.

MFs	Interval
SD	[−1.00, −0.40]
MD	[−0.60, −0.20]
LD	[−0.50, 0.00]
Z	[−0.20, 0.20]
LG	[0.00, 0.40]
MGH	[0.20, 0.60]
HG	[0.40, 1.00]

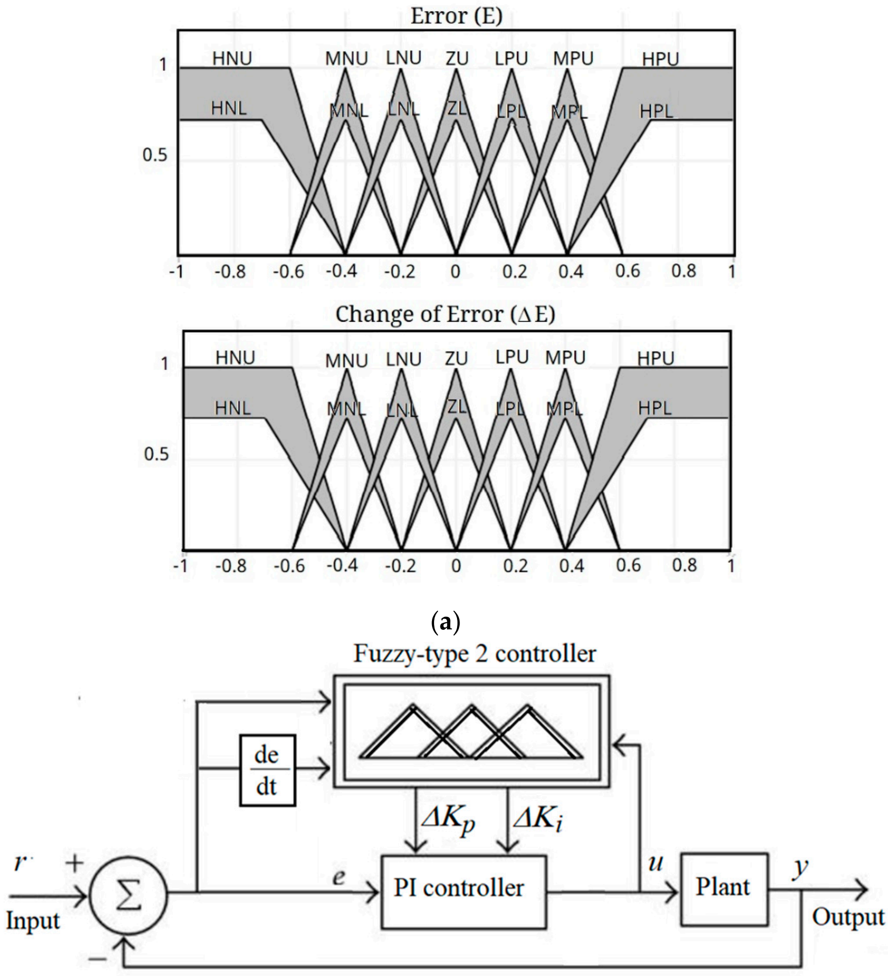

(**b**)

Figure 4. Fuzzy type 2 scheme: (**a**). Membership Functions for input. (**b**) Structure of the proposed controller.

Table 2. Fuzzy controllers rules.

ΔE	**E**						
	HN	**MN**	**LN**	**Z**	**LP**	**MP**	**HP**
HN	SD	SD	SD	SD	MD	LD	Z
MN	SD	SD	SD	MD	LD	Z	LG
LN	SD	SD	MD	LD	Z	LG	MGH
Z	SD	MD	LD	Z	LG	MGH	HG
LP	MD	LD	Z	LG	MGH	HG	HG
MP	LD	Z	LG	MGH	HG	HG	HG
HP	Z	LG	MGH	HG	HG	HG	HG

In Figure 4b, the system's error and change in error are initially fuzzified in accordance with their membership functions in the design of the fuzzy PI controller. The fuzzy reasoning is then used to calculate the membership degree for the PI controller's gain variations ΔK_p and ΔK_i. Moreover, the proportional and integral gains of the PI controller are adjusted by the defuzzified ΔK_p and ΔK_i.

5. Simulations and Experimental Results

5.1. Simulation Results

The MATLAB/SimPowerSystems Toolbox 2021a tests and simulates the suggested single-phase grid connected to the MG system with a near unity power factor. Figure 1 was implemented and tested to verify the robustness of the proposed control. The proposed nearly unity power factor grid connected to the MG system comprises a line filter, single-phase uncontrolled rectifier, and boost dc–dc converter. The DC-DC boost converter shown in Figure 3 was controlled using Fuzzy type 2 controllers. Two cascade control loops were designed. The inner controller is the current, and the outer control is the DC link voltage. Both controllers are PI-Fuzzy type 2. Two test cases were achieved. The gains of the autotuned PI controllers for the voltage and current loops were K_p = 0.361 and K_i = 1.452, respectively, for the voltage loop, K_p = 11.325 and K_i = 119.732 for the current loop.

When an error occurs, the PI controller produces a dc value. A sawtooth signal is compared to the dc signal. The combined pulse width modulation of these two signals is then fed into the transistor driving circuit, which is tailored to the specifics of that circuit.

The system was tested against nonlinear loads such as inverters, which adversely affect the system's power factor. In Case (1), the system given in Figure 2 was tested with a step change in the DC link voltage. Auto-tune PI controllers (conventional), Fuzzy type 1, and the suggested Fuzzy type 2 regulate the dc boost chopper. The source voltage and current for the three-control techniques and their respective source current spectrum are given. In Case (2), the system proposed in Figure 2 was tested against step change in the AC load (load increase and decrease). The DC link voltage, the source current, and the source current spectrums are shown. The proposed controllers were compared with Fuzzy type 1 and conventional controllers. The proposed Fuzzy type 2 controllers are advantageous compared to the other two techniques.

5.1.1. Case (1): Step Change in the DC Link Voltage

Figure 5 depicts the DC link voltage during system startup, a step increase in the DC link voltage from 400 to 600 V at t = 0.6 s, and a step decrease in the DC link voltage from 600 V to 500 V at t = 1 s. The proposed DC link voltage controller was compared to the conventional and Fuzzy type 1 controllers. The proposed DC link voltage controller outperformed the Fuzzy type 1 and conventional controllers regarding the system performance parameters. Figure 6 shows the inverter (load) voltage, current, and source voltage and current for the proposed system when the three control techniques were implemented during the step-up in the DC link voltage: Figure 6a for the conventional controller, Figure 6b for Fuzzy type 1, and Figure 6c for the proposed controller. Figure 7 shows the inverter (load) voltage, current, and source voltage and current for the proposed system when the three control techniques were implemented during the step down in the DC link voltage: Figure 7a for the conventional controller, Figure 7b for Fuzzy type 1, and Figure 7c for the proposed controller. The source current and its spectrum for the three control methods are given in Figure 8, where Figure 8a,d,g shows the conventional controller, Figure 8b,e,h for Fuzzy type 1, and Figure 8c,f,i for the proposed controller. The total harmonic distortion (THD), displacement factor, power factor, and whether it agrees or disagrees with IEEE 1547 standards are illustrated in Table 3. From Table 3, the proposed controller had the nearest unity power factor and agreed with the IEEE 1547 standards.

Table 3. Output memberships.

	Total Harmonic Distortion (%)	Displacement Factor (cos θ)	Power Factor	Agree or Disagree with IEEE 1547 Standards?
Conventional (auto-tune)	6.233	0.954	0.9521	Disagree
Fuzzy type 1	5.314	0.973	0.9716	Disagree
Proposed	3.212	0.997	0.9965	Agree

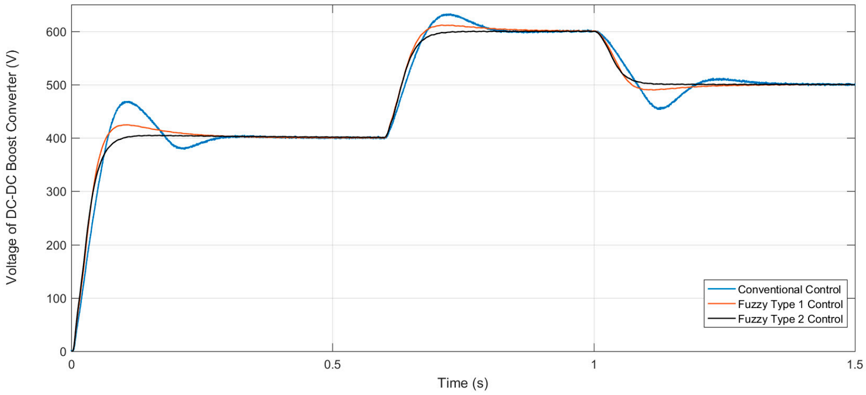

Figure 5. Start up, step increase, and step decrease for the DC link voltage using the three control techniques.

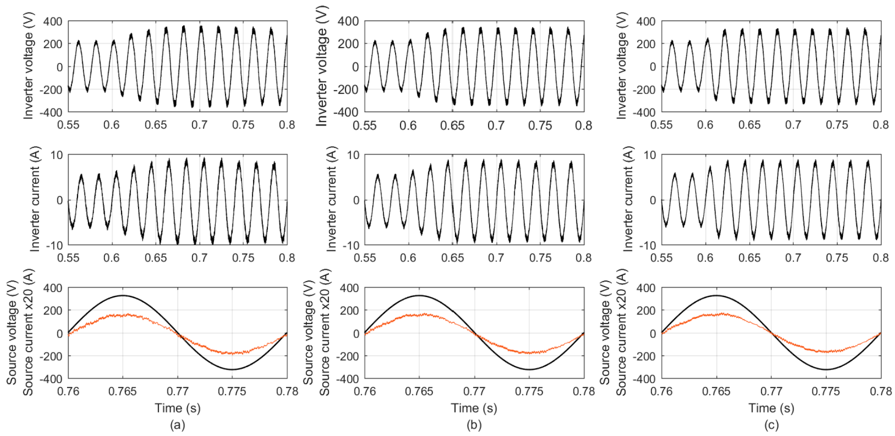

Figure 6. Inverter (Load) voltage and current, source voltage, and current for the three control techniques during the step increase of the DC link voltage: (**a**) autotuned (conventional) PI, (**b**) Fuzzy type 1 controller, and (**c**) Fuzzy type 2 controller. The black line is the voltage, the red line is the current. The red line represents the boarder line in IEEE Standard 1547 and it wtitten just above the red line.

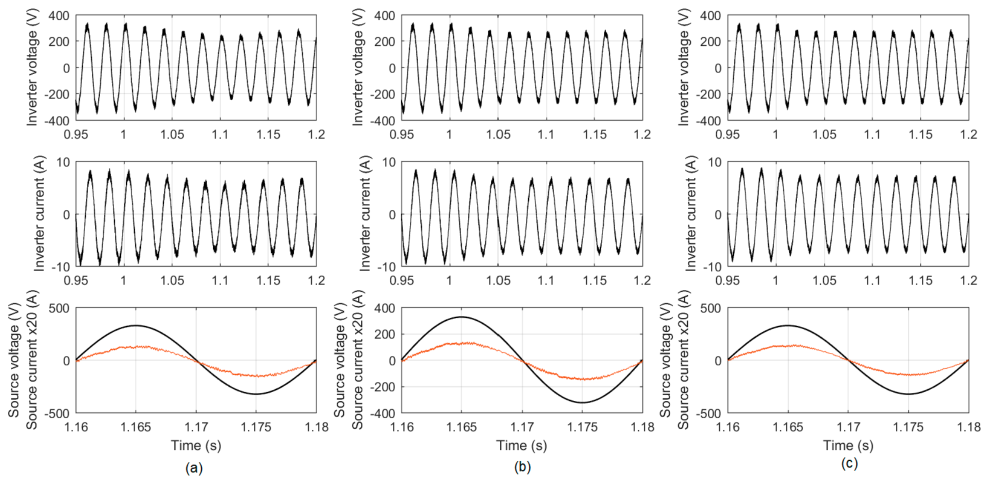

Figure 7. Inverter (Load) voltage and current, source voltage and current for the three control techniques during step decrease of the DC link voltage: (**a**) autotuned (conventional) PI, (**b**) Fuzzy type 1 controller, and (**c**) Fuzzy type 2 controller. The black line is the voltage, the red line is the current. The red line represents the boarder line in IEEE Standard 1547 and it wtitten just above the red line.

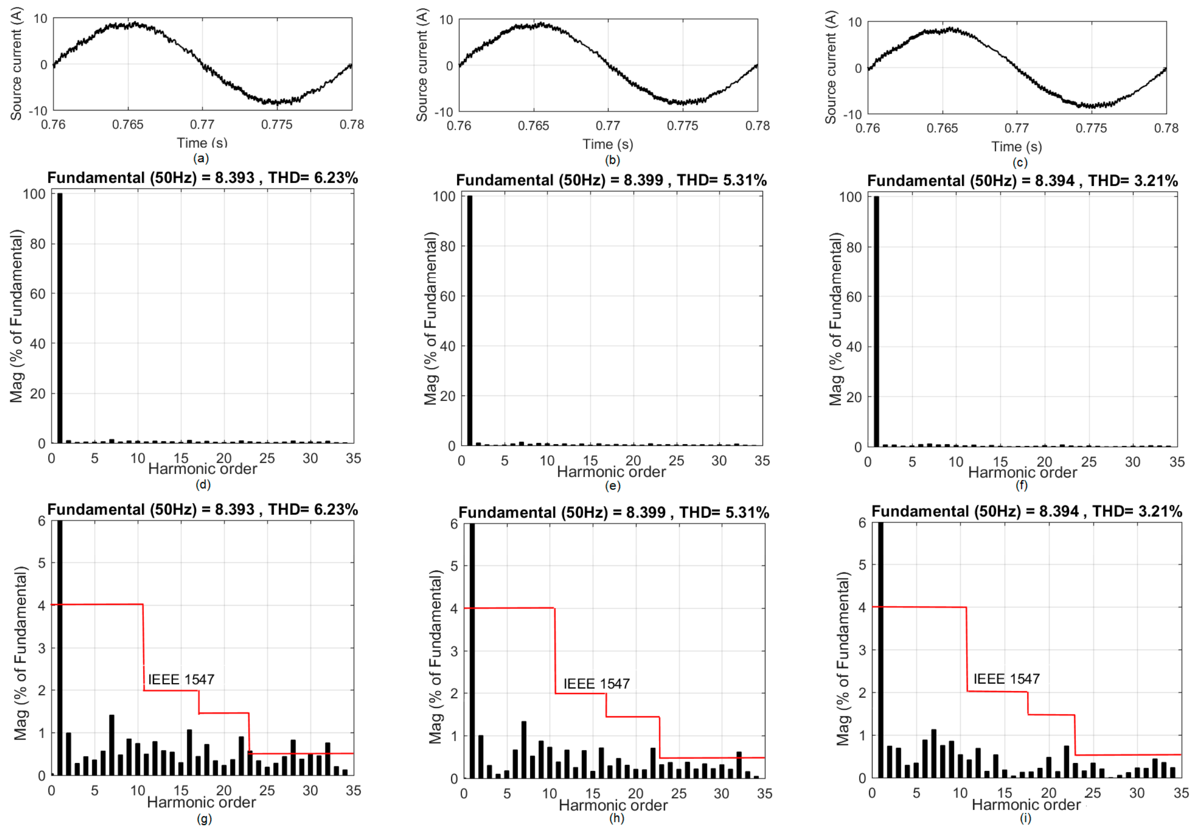

Figure 8. Source of the grid current and its spectrum for the three control techniques. (**a**,**d**,**g**) conventional method, (**b**,**e**,**h**) Fuzzy type 1 method, and (**c**,**f**,**i**) the proposed method.

5.1.2. Case (2): Step Change in the Load

Figure 9 illustrates a step change in the MG's AC load side. Load 1 with p = 2.5 kW and Q = 1.2 kVAR (S = 2.7 kVA = 58%) was stepped up to Load 2 with p = 4.2 kW and Q = 2 kVAR (S = 4.65 kVA = 100%) and then stepped back down to Load 1. The DC link voltage, source current, and one cycle of the source voltage and source current for the three control techniques are shown in Figure 9a–d, respectively. Figure 10 depicts one source's current cycle and its spectrum for the three control approaches when Load 2 was applied. The conventional technique is depicted in Figure 10a,d, the Fuzzy type 1 method is depicted in Figure 10b,e, and the proposed control method is depicted in Figure 10b,e,c,f. Table 4 shows the THD, displacement factor, power factor, and whether it agrees or disagrees with the IEEE 1547 standards. According to Table 4, the proposed controller had the closest to unity power factor and adhered to the IEEE 1547 standards.

Table 4. Summary of the simulation results.

	Total Harmonic Distortion (%)	Displacement Factor (cos θ)	Power Factor	Agree or Disagree with IEEE 1547 Standards?
Conventional (auto-tune)	7.16	0.949	0.9466	Disagree
Fuzzy type 1	5.35	0.967	0.9654	Disagree
Proposed	2.09	0.991	0.9905	Agree

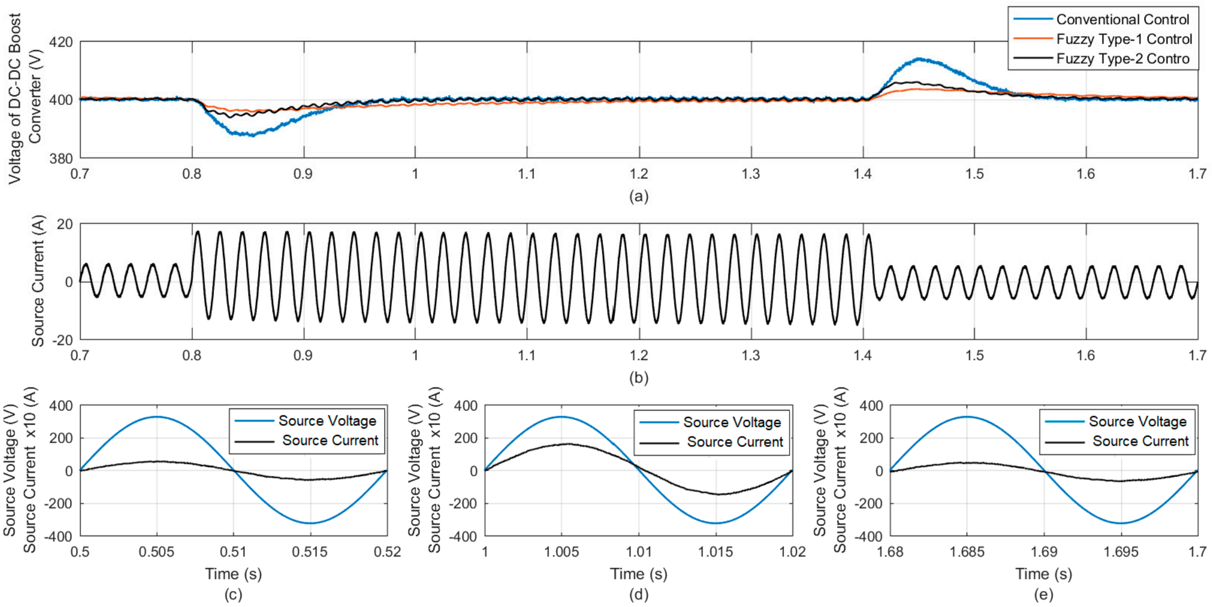

Figure 9. Step change from Load 1 to Load 2 and back to Load 1 for the three control techniques: (**a**) DC link voltage, (**b**) source current, (**c**) one cycle for the source voltage and current with conventional method, (**d**) one cycle for the source voltage and current with Fuzzy type 1 method, and (**e**) one cycle for the source voltage and current with the proposed method.

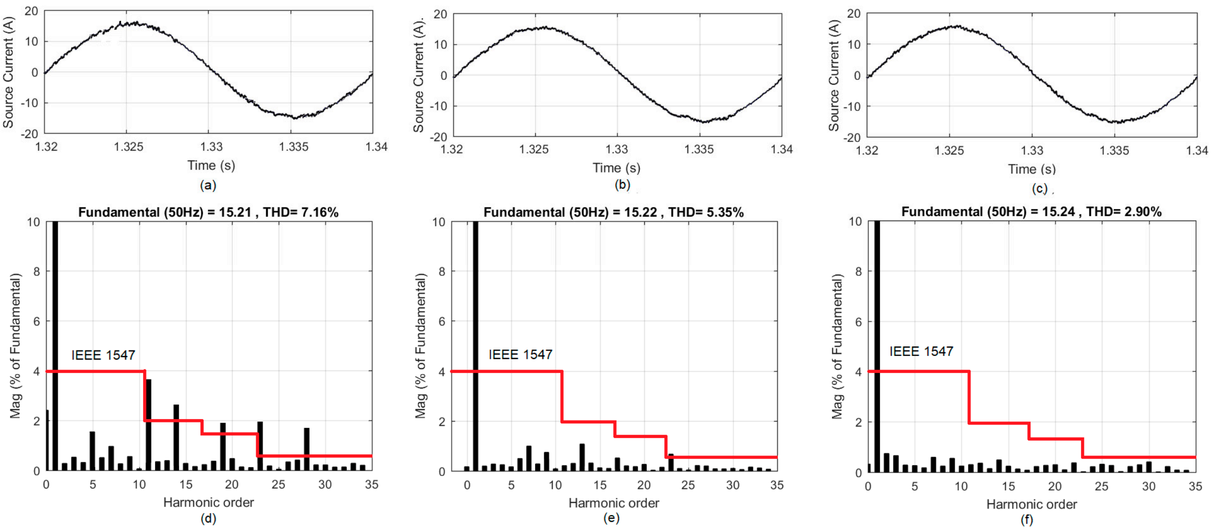

Figure 10. One source current cycle and its spectrum when Load 2 was applied for the three control techniques: (**a**,**d**) conventional method, (**b**,**e**) Fuzzy type 1, and (**c**,**f**) the proposed method.

5.2. Experimental Results

As illustrated in Figure 11a,b, the proposed techniques were implemented on the dSPACE 1104 platform with a sampling frequency of 10 kHz. The grid was simulated in real-time within the dSPACE, and the grid voltage was fed to the proposed system under review. The performance variables were monitored using a digital scope and the dSPACE Digital to Analog converters D/A with 16-bit resolution. Two test cases were executed. In Case (1), a step change in the DC link voltage was used to test the system shown in Figure 12. Stepped voltage for the DC link ranged from 400 V to 600 V. The proposed controller's performance parameters for the DC link voltage response were as follows: settling time (t_s), rise time (t_r), and maximum percentage overshoot (3.35%). The DC link voltage proposed controller had a swift response consistent with the simulation results.

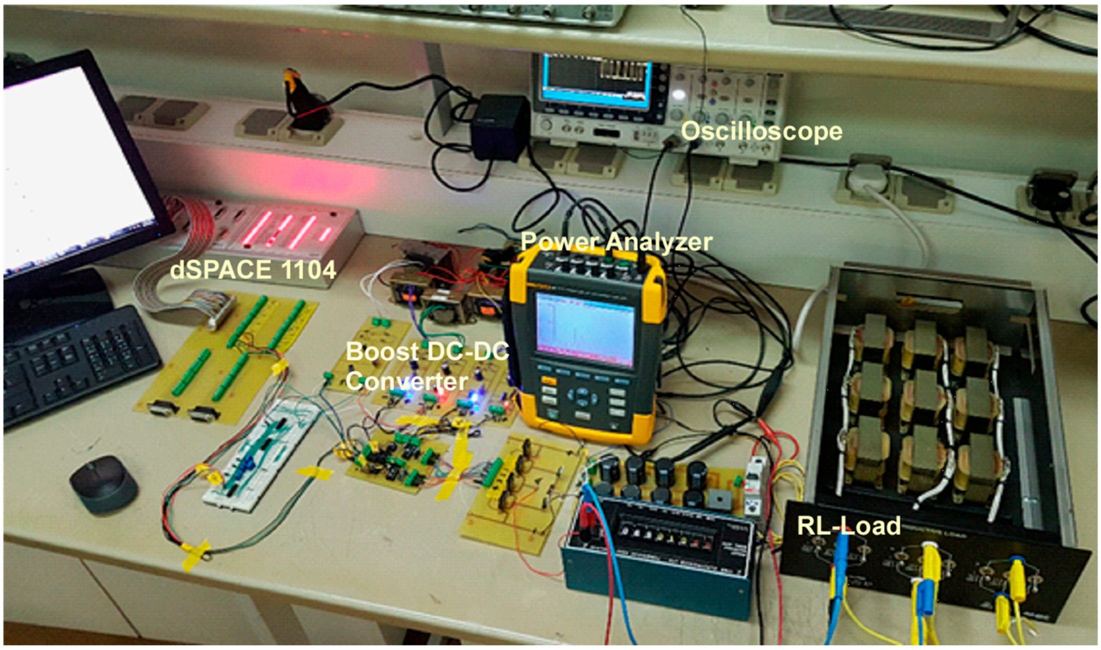

(**a**)

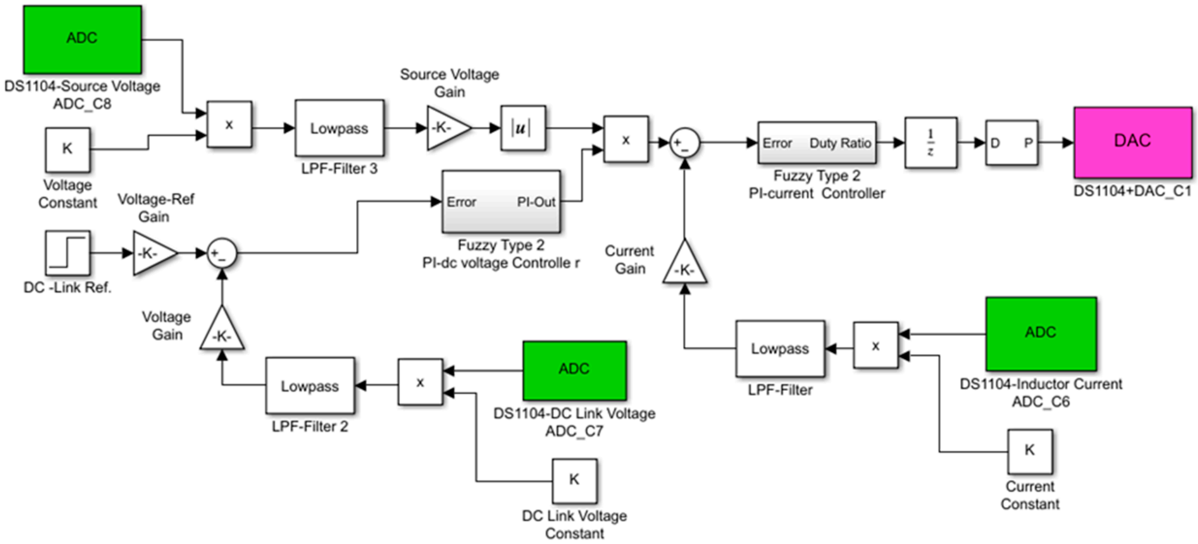

(**b**)

Figure 11. The proposed system's experimental setup: (**a**) hardware implementation, and (**b**) Simulink model for controlling the DS1104 board.

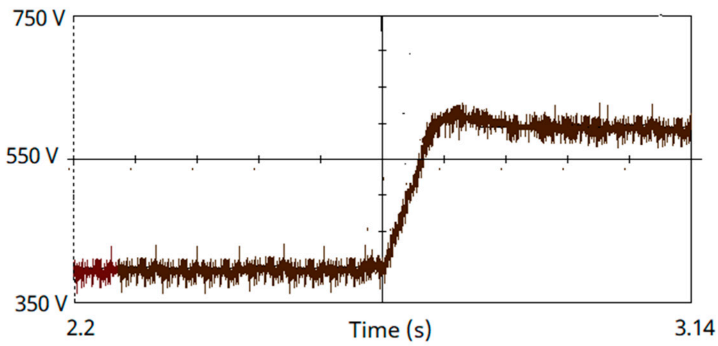

Figure 12. Step change in the dc link voltage from 400 to 600 V.

In Case (2), the system was tested when the ac load was stepped from 0% to 100% and then returned to 0% from the full load value. Figure 13 shows the source current and DC link voltage. Figure 14 depicts the source voltage and current during step changes in the AC load side. The source voltage and current are shown in Figure 14a during 100% AC load, Figure 14b during switching from 0 to 100% AC load at t = 0.767 s, and Figure 14c during switching from 100 to 0% AC load at t = 2.417 s. Figure 15 shows that the displacement angle between the source voltage and current was less than 8°, resulting in a displacement factor of about 0.990 when applying a 100% AC load. Figure 16 depicts the source current spectrum when applying a 100% AC load. The THD was 3.11%, which made the power factor 0.972. Case (2) outcomes will adhere to the simulation outcomes presented in Table 4.

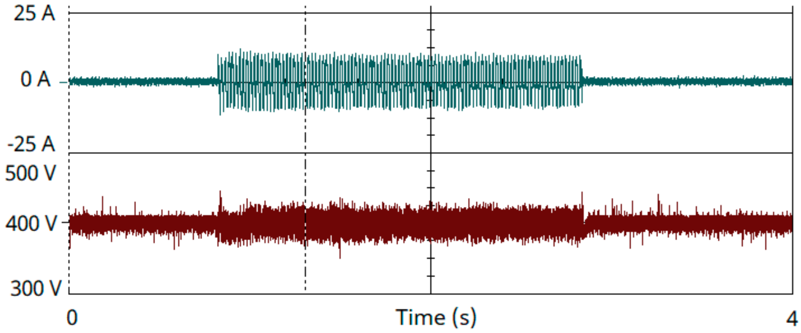

Figure 13. The source current and the DC link voltage during a step change in the ac loads from 0% to 100%.

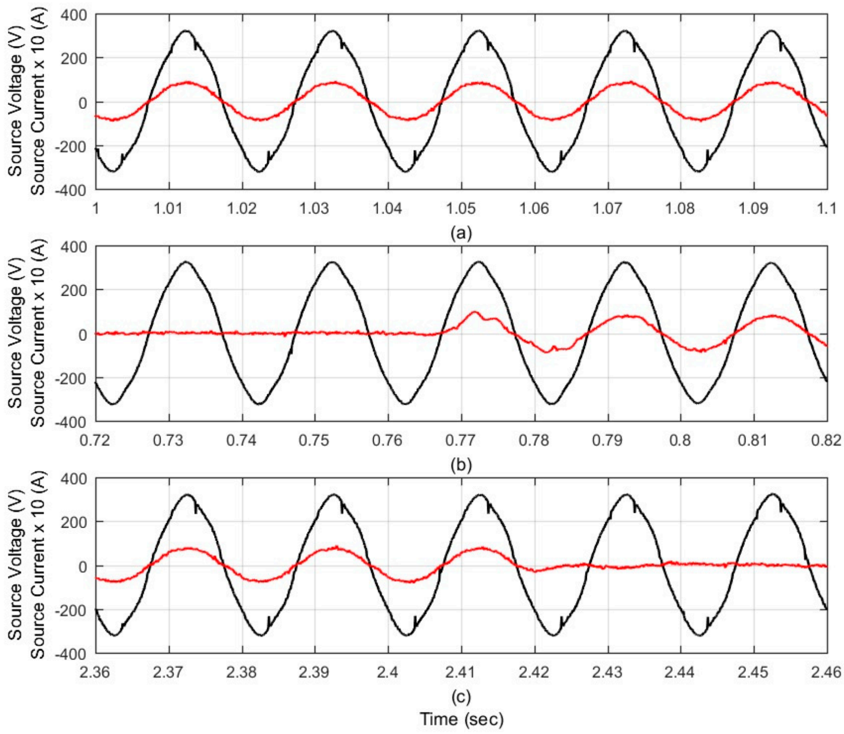

Figure 14. The source voltage and current during step changes in the ac load side: (**a**) during 100% load, (**b**) from 0 to 100% load, and (**c**) from 100 to 0% load. The black line is the voltage and the red line is the current.

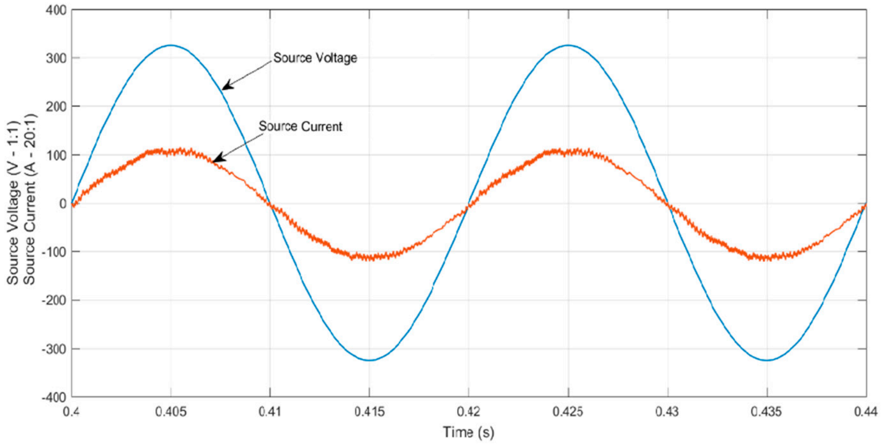

Figure 15. The source voltage and current of the single-phase grid.

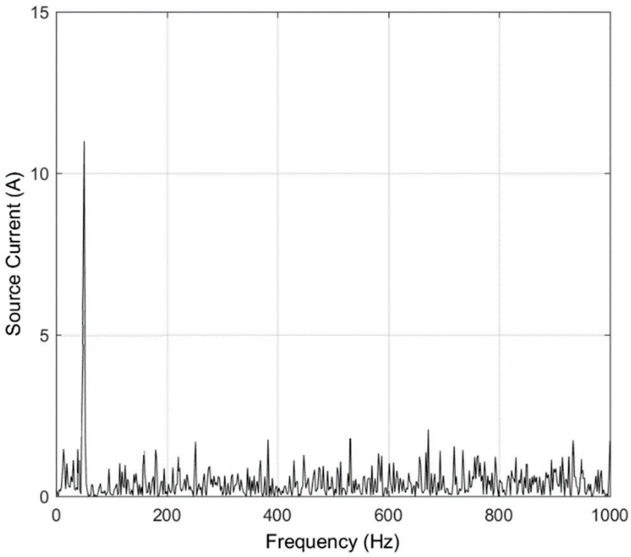

Figure 16. Source current spectrum when 100% AC load is applied.

Simulation results were generated when the AC load side alternated between two loads. Load 1 with p = 2.5 kW and Q = 1.2 kVAR (S = 2.7 kVA = 58%) was increased to Load 2 with p = 4.2 kW and Q = 2 kVAR (S = 4.65 kVA = 100%). In the experimental work, the transitioning between two loads was from 0% to 100%, which was more severe than in the simulation, demonstrating that the system is well-designed to handle this severe change.

Analyses of the simulation and experimental results were carried out at 100% load capacity (full load). Calculations of the harmonic distortion, displacement factor, and power factor were made at full load for the findings of both the simulation and the experiment.

Comparing the simulations to the experimental results using the proposed controller yielded the data in Tables 5 and 6.

Table 5. DC-link voltage performance parameters in the simulation compared to the experimental results.

	Simulation	Experimental
Settling Time (s)	0.114	0.13
Overshoot (%)	1.07	3.35

Table 6. Source current performance parameters in the simulation compared to the experimental results.

	Simulation	Experimental
Displacement factor	0.991	0.972
Total Harmonic Distortion	2.09	3.11
Power Factor	0.9905	0.972
IEEE 1547 Standards	AGREE	AGREE

5.3. Practical Implications

Increasing the switching frequency does not have the desired effect of decreasing the necessary filter attenuation. The attenuation of a filter can be improved by around 10 dB by increasing the switching frequency from 10 kHz to 80 kHz. However, the switching losses will increase by a factor of 8. Therefore, it is desirable to reduce the noise generated. The noise produced by the input capacitor is proportional to the current ripple. Noise can be reduced by lowering the current ripple in the boost inductor. Continuous mode operating produces the least amount of noise. Another method of noise reduction is variable frequency operation. This spreads the noise spectra over a wider frequency range, reducing the peak loudness of the noise and thus the amount of filter attenuation required. Furthermore, it will complicate the control method in its practical implementation.

We settled on a fixed switching frequency of 10 kHz to tackle this issue in the experimental work. This represents a compromise between the switching losses and the attenuation caused by the filter.

In a large number of power factor applications, the voltage error amplifier cannot be used to compensate for input supply voltage fluctuations. This is because the output of the PFC is not pure DC; a small quantity of ripple still exists on top of the DC signal, which cannot be eradicated with a realistically sized bulk capacitor at high voltage and current levels. This ripple was slightly out of phase with the main signal that had been half-wave corrected. Therefore, the voltage error amplifier's input must be low-pass filtered to get rid of the ripple.

Typically, in experimental work, this filter is designed to have a crossover frequency of approximately 20 Hz to eliminate sufficient experimental noise and enable the error amplifier to function properly.

6. Conclusions

The proposed Fuzzy type 2 controllers improved the power factor of single-phase MGs in both the simulations using MATLAB/Simulink and experiments using a 10-kHz-sampling dSPACE platform. Step changes in the DC link voltage and AC load were examined (increase and decrease). The simulations and experimental results showed that the suggested Fuzzy type 2 controller outperformed the other two systems in the dynamic response, steady-state error, and compliance with the power quality standards. In the case of the DC-link voltage step change, the proposed controller reduced the THD by 40.7% and improved the power factor by 4.56%. In the case of the AC-load step change, the proposed technique reduced the THD by 51.5 % and improved the power factor by about 4.73%. In both cases, the results comply with the requirements of the power quality standards. Unlike meta-heuristic optimization approaches, this paper predicted the FLC parameters using deterministic optimization, ensuring an optimal solution. Additionally, the FLC technique was used to address power quality concerns using DC microgrids, which is uncommon in the literature. The proposed technique can be easily applied to various systems including various structures of MGs and other power system applications.

Investigation of the influence of nested loop controllers on each individual loop could be handled in a separate paper, which could be an extension of the current research.

The sensitivity of the proposed controller to the parameter variations was not studied, which could be the direction of further research. However, the controller design should involve the disturbance rejection capability by considering other methods such as invariant-set and H_∞.

Author Contributions: Conceptualization, H.A. and E.H.E.B.; Methodology, E.H.E.B., A.M.I. and H.A.; Software, A.M.I., H.A. and E.H.E.B.; Validation, M.D.S., E.H.E.B., A.M.I. and H.A.; Formal analysis, M.D.S., E.H.E.B., A.M.I. and H.A.; Investigation, M.D.S., E.H.E.B., A.M.I. and H.A.; Resources, H.A. and E.H.E.B.; Data curation, M.D.S., E.H.E.B., A.M.I. and H.A.; Writing—original draft preparation, M.D.S., E.H.E.B., A.M.I. and H.A.; Writing—review and editing, M.D.S., E.H.E.B., A.M.I. and H.A.; Visualization, M.D.S., E.H.E.B., A.M.I. and H.A.; Supervision, E.H.E.B. and A.M.I. All authors have read and agreed to the published version of the manuscript.

Funding: This research received no external funding.

Institutional Review Board Statement: Not applicable.

Informed Consent Statement: Not applicable.

Data Availability Statement: Not applicable.

Conflicts of Interest: The authors declare no conflict of interest.

Nomenclature

FLC	Fuzzy logic control
HG	High growth
HN	High negative
HP	High positive
LD	Low drop
LG	Low growth
LN	Low negative
LP	Low positive
MF	Member function
MD	Medium drop
MGH	Medium growth
MG	Microgrid
MN	Medium negative
MP	Medium positive
PI	Proportional integral
PWM	Pulse-width modulation
SD	Steep drop
THD	Total harmonic distortion
Z	Zero
i_{b}	Rectified current
i_{dc}	DC-load current
v_{b}	Rectified voltage
V_{dc}	DC-link voltage

References

1. Cavus, M.; Allahham, A.; Adhikari, K.; Zangiabadi, M.; Giaouris, D. Energy Management of Grid-Connected Microgrids Using an Optimal Systems Approach. *IEEE Access* **2023**, *11*, 9907–9919. [CrossRef]
2. Liu, Q.; Caldognetto, T.; Buso, S. Review and Comparison of Grid-Tied Inverter Controllers in Microgrids. *IEEE Trans. Power Electron.* **2020**, *35*, 7624–7639. [CrossRef]
3. Saxena, A.; Patil, G.M.; Agarwal, N.K.; Singh, A.; Prakash, A.; Sharma, K. Environmental and Social Aspects of Microgrid Deployment—A Review. In Proceedings of the 2021 IEEE 8th Uttar Pradesh Section International Conference on Electrical, Electronics and Computer Engineering, UPCON 2021, Dehradun, India, 11–13 November 2021. [CrossRef]
4. Singh, G.; Cooke, T.; Howe, W. Impact of Microgrids on Power Factor measurements. In Proceedings of the International Conference on Harmonics and Quality of Power, ICHQP, Dubai, United Arab Emirates, 6–7 July 2020. [CrossRef]
5. Kumar, D.; Zare, F. A Comprehensive Review of Maritime Microgrids: System Architectures, Energy Efficiency, Power Quality, and Regulations. *IEEE Access* **2019**, *7*, 67249–67277. [CrossRef]

6. How Power Factor & Induction Motors Can Impact the Bottom Line | Pumps & Systems. Available online: https://www.pumpsandsystems.com/how-power-factor-induction-motors-can-impact-bottom-line (accessed on 12 February 2023).
7. Singh, B.; Bhuvaneswari, G.; Garg, V. Power-Quality Improvements in Vector-Controlled Induction Motor Drive Employing Pulse Multiplication in AC–DC Converters. *IEEE Trans. Power Deliv.* **2006**, *21*, 1578–1586. [CrossRef]
8. Metwaly, M.K.; Azazi, H.Z.; Deraz, S.A.; Dessouki, M.E.; Zaky, M.S. Power factor correction of three-phase PWM AC chopper fed induction motor drive system using HBCC technique. *IEEE Access* **2019**, *7*, 43438–43452. [CrossRef]
9. Jibhakate, C.N.; Chaudhari, M.A.; Renge, M.M. Reactive Power Compensation Using Induction Motor Driven by Nine Switch AC-DC-AC Converter. *IEEE Access* **2017**, *6*, 1312–1320. [CrossRef]
10. Özdemir, A.; Erdem, Z. Double-loop PI controller design of the DC-DC boost converter with a proposed approach for calculation of the controller parameters. *Proc. Inst. Mech. Eng. Part I J. Syst. Control Eng.* **2017**, *232*, 137–148. [CrossRef]
11. Cortes, D.; Alvarez, J. Robust sliding mode control for the boost converter. In Proceedings of the International Power Electronics Congress—CIEP, Guadalajara, Mexico, 24 October 2002; pp. 208–212. [CrossRef]
12. Rodriguez, M.; Arcos-Aviles, D.; Martinez, W. Fuzzy logic-based energy management for isolated microgrid using meta-heuristic optimization algorithms. *Appl. Energy* **2023**, *335*, 120771. [CrossRef]
13. Buswig, Y.M.; Othman, A.-K.; Julai, N.; Yi, S.S.; Mulyo Utomo, W.; Siang, A.J.L.M. Voltage Tracking of a Multi-Input Interleaved Buck-Boost DC-DC Converter Using Artificial Neural Network Control. *J. Telecommun. Electron. Comput. Eng. JTEC* **2018**, *10*, 29–32. Available online: https://jtec.utem.edu.my/jtec/article/view/3822 (accessed on 9 March 2023).
14. Mattavelli, P.; Rossetto, L.; Spiazzi, G.; Tenti, P. General-purpose fuzzy controller for DC-DC converters. *IEEE Trans. Power Electron.* **1997**, *12*, 79–86. [CrossRef]
15. Ismail, N.F.N.; Musirin, I.; Baharom, R.; Johari, D. Fuzzy logic controller on DC/DC boost converter. In Proceedings of the PECon2010—2010 IEEE International Conference on Power and Energy, Kuala Lumpur, Malaysia, 29 Novemeber–1 December 2010; pp. 661–666. [CrossRef]
16. Birkin, P.A.; Garibaldi, J.M. A comparison of Type-1 and Type-2 fuzzy controllers in a micro-robot context. *IEEE Int. Conf. Fuzzy Syst.* **2009**, *2009*, 1857–1862. [CrossRef]
17. Castillo, O.; Amador-Angulo, L.; Castro, J.R.; Garcia-Valdez, M. A comparative study of type-1 fuzzy logic systems, interval type-2 fuzzy logic systems and generalized type-2 fuzzy logic systems in control problems. *Inf. Sci.* **2016**, *354*, 257–274. [CrossRef]
18. Dimitroulis, P.; Alamaniotis, M. A fuzzy logic energy management system of on-grid electrical system for residential prosumers. *Electr. Power Syst. Res.* **2021**, *202*, 107621. [CrossRef]
19. Vivas, F.; Segura, F.; Andújar, J. Fuzzy logic-based energy management system for grid-connected residential DC microgrids with multi-stack fuel cell systems: A multi-objective approach. *Sustain. Energy Grids Netw.* **2022**, *32*, 100909. [CrossRef]
20. Aviles, D.A.; Guinjoan, F.; Barricarte, J.; Marroyo, L.; Sanchis, P.; Valderrama, H. Battery management fuzzy control for a grid-tied microgrid with renewable generation. In Proceedings of the IECON 2012—38th Annual Conference on IEEE Industrial Electronics Society, Montreal, QC, Canada, 25–28 October 2012; pp. 5607–5612. [CrossRef]
21. Arcos-Aviles, D.; Pacheco, D.; Pereira, D.; Garcia-Gutierrez, G.; Carrera, E.V.; Ibarra, A.; Ayala, P.; Martínez, W.; Guinjoan, F. A Comparison of Fuzzy-Based Energy Management Systems Adjusted by Nature-Inspired Algorithms. *Appl. Sci.* **2021**, *11*, 1663. [CrossRef]
22. Awad, H.; Bayoumi, E.H.; Soliman, H.M.; Ibrahim, A.M. Invariant-set design of robust switched trackers for bidirectional power converters in hybrid microgrids. *Ain Shams Eng. J.* **2023**, *2023*, 102123. [CrossRef]
23. Awad, H.; Bayoumi, E.H.E.; Soliman, H.M.; De Santis, M. Robust Tracker of Hybrid Microgrids by the Invariant-Ellipsoid Set. *Electronics* **2021**, *10*, 1794. [CrossRef]
24. Tarasiuk, T.; Jayasinghe, S.G.; Gorniak, M.; Pilat, A.; Shagar, V.; Liu, W.; Guerrero, J.M. Review of Power Quality Issues in Maritime Microgrids. *IEEE Access* **2021**, *9*, 81798–81817. [CrossRef]
25. Bonaldo, J.P.; De Souza, V.A.; Alonso, A.M.D.S.; Arenas, L.D.O.; Marafao, F.P.; Paredes, H.K.M. Adaptive Power Factor Regulation Under Asymmetrical and Non-Sinusoidal Grid Condition With Distributed Energy Resource. *IEEE Access* **2021**, *9*, 140487–140503. [CrossRef]
26. Razmi, D.; Lu, T.; Papari, B.; Akbari, E.; Fathi, G.; Ghadamyari, M. An Overview on Power Quality Issues and Control Strategies for Distribution Networks With the Presence of Distributed Generation Resources. *IEEE Access* **2023**, *11*, 10308–10325. [CrossRef]
27. Soliman, H.M.; Saleem, A.; Bayoumi, E.H.E.; De Santis, M. Harmonic Distortion Reduction of Transformer-Less Grid-Connected Converters by Ellipsoidal-Based Robust Control. *Energies* **2023**, *16*, 1362. [CrossRef]
28. Gayatri, M.; Parimi, A.M. Mitigation of supply & load side disturbances in an AC Microgrid using UPQC. In Proceedings of the 2016 IEEE 6th International Conference on Power Systems, ICPS 2016, New Delhi, India, 4–6 March 2016. [CrossRef]
29. Rebollal, D.; Carpintero-Rentería, M.; Santos-Martín, D.; Chinchilla, M. Microgrid and Distributed Energy Resources Standards and Guidelines Review: Grid Connection and Operation Technical Requirements. *Energies* **2021**, *14*, 523. [CrossRef]
30. *ARCONEL 003-2018*; Microgeneración Fotovoltaica para Autoabastecimiento de Consumidores Finales de Energía Eléctrica. Agencia de Regulación y Control de Electricidad (ARCONEL): Quito, Ecuador, 2018.
31. Pomilio, J.A.; Bonaldo, J.P.; Morales-Paredes, H.K.; Tenti, P. About power factor and THDi in the smart micro-grid scenario. In Proceedings of the 2015 IEEE 13th Brazilian Power Electronics Conference and 1st Southern Power Electronics Conference (COBEP/SPEC), Fortaleza, Brazil, 29 November–2 December 2015; pp. 1–5. [CrossRef]

32. Kow, K.W.; Wong, Y.W.; Rajkumar, R.K.; Rajkumar, R.K. Power Quality Analysis for PV Grid Connected System Using PSCAD/EMTDC. *Int. J. Renew. Energy Res.* **2015**, *5*, 121–132.
33. Li, L.; Sun, Y.; Liu, Y.; Han, H.; Ye, H.; Su, M.; Shi, G. Power factor consistency control for decentralized power sharing in islanded AC microgrids with cascaded inverters. In Proceedings of the IECON 2017—43rd Annual Conference of the IEEE Industrial Electronics Society, Beijing, China, 29 October–1 November 2017; pp. 1435–1440. [CrossRef]
34. Hashempour, M.M.; Lee, T.-L. Integrated power factor correction and voltage fluctuation mitigation of microgrid using STATCOM. In Proceedings of the 2017 IEEE 3rd International Future Energy Electronics Conference and ECCE Asia (IFEEC 2017—ECCE Asia), Kaohsiung, Taiwan, 3–7 June 2017; pp. 1215–1219. [CrossRef]
35. Varma, R.K.; Siavashi, E.M.; Das, B.; Sharma, V. Real-Time Digital Simulation of a PV solar system as STATCOM (PV-STATCOM) for voltage regulation and power factor correction. In Proceedings of the 2012 IEEE Electrical Power and Energy Conference, Champaign, IL, USA, 24–25 February 2012; pp. 157–163. [CrossRef]
36. Lim, S.; Otten, D.M.; Perreault, D.J. New AC–DC Power Factor Correction Architecture Suitable for High-Frequency Operation. *IEEE Trans. Power Electron.* **2016**, *31*, 2937–2949. [CrossRef]
37. Ullah, K.M.S.; Roomi, M.M.; Tariq, M.; Zhao, B. A Unity Power Factor Rectifier based Dynamic Voltage Restorer for Microgrid Applications. In Proceedings of the 2020 IEEE 17th India Council International Conference (INDICON), New Delhi, India, 10–13 December 2020; pp. 1–6.
38. Rahmani, S.; Rezaei-Zare, A.; Rezaei-Zare, M.; Hooshyar, A. Voltage and Frequency Recovery in an Islanded Inverter-Based Microgrid Considering Load Type and Power Factor. *IEEE Trans. Smart Grid* **2019**, *10*, 6237–6247. [CrossRef]
39. Kaushal, J.; Basak, P. Power quality control based on voltage sag/swell, unbalancing, frequency, THD and power factor using artificial neural network in PV integrated AC microgrid. *Sustain. Energy Grids Netw.* **2020**, *23*, 100365. [CrossRef]
40. Anwar, S.; Elrayyah, A.; Sozer, Y.; Anwar, S. Efficient single phase power factor improvement strategy for microgrid operation. In Proceedings of the 2014 IEEE Applied Power Electronics Conference and Exposition—APEC 2014, Fort Worth, TX, USA, 16–20 March 2014; pp. 972–977. [CrossRef]
41. Mohanty, S.; Pati, S.; Kar, S.K.; Lenka, L.R. Performance of Electric Spring Under Varying Non-Critical Load Power Factor in Isolated Microgrid. In Proceedings of the 2022 IEEE 2nd International Symposium on Sustainable Energy, Signal Processing and Cyber Security (iSSSC), Gunupur, Odisha, India, 15–17 December 2022; pp. 1–5. [CrossRef]
42. Martínez-Soto, R.; Castillo, O.; Aguilar, L.T. Type-1 and Type-2 fuzzy logic controller design using a Hybrid PSO–GA optimization method. *Inf. Sci.* **2014**, *285*, 35–49. [CrossRef]
43. Wu, D.; Mendel, J.M. Recommendations on designing practical interval type-2 fuzzy systems. *Eng. Appl. Artif. Intell.* **2019**, *85*, 182–193. [CrossRef]